Commun. Theor. Phys. **77** (2025) 045001 (11pp) https://doi.org/10.1088/1572-9494/ad8c27

Three-component soliton states in spinor $F=1$ Bose–Einstein condensates with $\mathcal{PT}$-symmetric generalized Scarf-II potentials

Zhang-Lei Han, Jun-Yi Lao, Jia-Rui Zhang and Yu-Jia Shen*

College of Science, China Agricultural University, Beijing 100083, China

E-mail: yjshen2018@cau.edu.cn

Received 23 April 2024, revised 22 September 2024
Accepted for publication 29 October 2024
Published 20 December 2024

Abstract

Introducing $\mathcal{PT}$-symmetric generalized Scarf-II potentials into the three-coupled nonlinear Gross–Pitaevskii equations offers a new way to seek stable soliton states in quasi-one-dimensional spin-1 Bose–Einstein condensates. In scenarios where the spin-independent parameter c_0 and the spin-dependent parameter c_2 vary, we use both analytical and numerical methods to investigate the three-coupled nonlinear Gross–Pitaevskii equations with $\mathcal{PT}$-symmetric generalized Scarf-II potentials. We obtain analytical soliton states and find that simply modulating c_2 may change the analytical soliton states from unstable to stable. Additionally, we obtain numerically stable double-hump soliton states propagating in the form of periodic oscillations, exhibiting distinct behavior in energy exchange. For further investigation, we discuss the interaction of numerical double-hump solitons with Gaussian solitons and observe the transfer of energy among the three components. These findings may contribute to a deeper understanding of solitons in Bose–Einstein condensates with $\mathcal{PT}$-symmetric potentials and may hold significance for both theoretical understanding and experimental design in related physics experiments.

Keywords: three-component soliton states, $\mathcal{PT}$-symmetric generalized Scarf-II potentials, Bose–Einstein condensates, Three-coupled nonlinear Gross–Pitaevskii equations

1. Introduction

The phenomenon of a marked increase in wave-like behavior occurs in atomic gases as temperatures decrease, leading to special physical properties such as superfluidity [1–3], superconductivity [4, 5], and quantum entanglement [6–8], is referred to as Bose–Einstein condensates (BECs). With the observation of spinor BECs in the gas of spin-1 Na^{23} atoms [9], interests in related theories are sparked, which drive the exploration of various new phenomena, including spin configurations [10, 11], quantum magnetization [12, 13], and the second-order Zeeman effect [14–16]. In recent years, methods involving time-dependent nonlinearity manipulated by Feshbach-resonance techniques have sparked research interest [17–20]. For instance, Feshbach-resonance is utilized to control scattering lengths, and numerical methods are employed to establish the complete stability of solitons [17]. Simultaneously, physical techniques enable control over the collapse and expansion in BECs [18]. Furthermore, methods for modulation of BEC systems involving external potentials with spatiotemporal dependencies have also been investigated [21–23]. Specifically, numerous studies focus on solitons in BECs or spinor BECs, with a primary focus on scenarios that only involve real external potential while a fraction further introduce gain-and-loss distribution manifested as imaginary component [24–26]. Moreover, there has been relatively scant research on modulating stable solitons in spinor BECs based on the concept of $\mathcal{PT}$-symmetry [27–30], i.e. external potential and gain-and-loss distribution must satisfy the parity conditions. $\mathcal{PT}$-symmetry was first proposed by Bender *et al* in 1998, and it has found significant applications in various fields including optics [31–34], matter waves [35, 36], magnetics [37, 38], acoustics [39, 40], and electronics [41, 42]. In dissipative systems, the $\mathcal{PT}$-symmetry of complex potentials

* Author to whom any correspondence should be addressed.

is a necessary condition for the existence of soliton families [43]. Despite the presence of gain and loss, the linear spectrum of the system can still be entirely real [44], allowing all linear modes to exhibit regular wave behavior as in conservative systems. Various $\mathcal{PT}$-symmetric potentials have been applied to BEC research since Klaiman *et al* proposed considering BECs in double-well potentials in 2008 [45], leading to an increasing number of studies on solitons in BECs [46–48].

The spinor BECs has $2F+1$ components. Governed by the variational principle, the evolution of the wave function in quasi-one-dimensional spin-1 BECs can be expressed using the three-coupled nonlinear Gross–Pitaevskii equations (GPEs) in the following form [49–53]:

$$\begin{aligned}
\mathrm{i}\hbar\partial_\tau\Psi_+ =& -\frac{\hbar^2}{2m}\partial_\zeta^2\Psi_+ + \hat{V}_+(\zeta)\Psi_+ + (b_0+b_2)(|\Psi_+|^2\\
&+|\Psi_0|^2)\Psi_+ + (b_0-b_2)|\Psi_-|^2\Psi_+ + b_2\Psi_0^2\Psi_-^*,\\
\mathrm{i}\hbar\partial_\tau\Psi_0 =& -\frac{\hbar^2}{2m}\partial_\zeta^2\Psi_0 + \hat{V}_0(\zeta)\Psi_0 + (b_0+b_2)(|\Psi_+|^2\\
&+|\Psi_-|^2)\Psi_0 + b_0|\Psi_0|^2\Psi_0 \quad + \quad 2b_2\Psi_0^*\Psi_+\Psi_-,\\
\mathrm{i}\hbar\partial_\tau\Psi_- =& -\frac{\hbar^2}{2m}\partial_\zeta^2\Psi_- + \hat{V}_-(\zeta)\Psi_- + (b_0+b_2)(|\Psi_0|^2\\
&+|\Psi_-|^2)\Psi_- + (b_0-b_2)|\Psi_+|^2\Psi_- + b_2\Psi_0^2\Psi_+^*,
\end{aligned} \tag{1}$$

where $\mathbf{\Psi}=(\Psi_+,\Psi_0,\Psi_-)^{\mathrm{T}}$, $\Psi_j(\zeta,\tau)$ $(j=+,0,-)$ is the wave function of ζ, τ which describe the transverse coordinate and propagation time respectively. And the asterisk stands for the complex conjugate, $\hbar$ is the reduced Planck constant, m is the atomic mass and $\hat{V}_j(\zeta)$ $(j=+,0,-)$ stands for the real external trap potential. Here, the mean-field coupling constants b_0 and b_2, which denote the interactions among the three components $\Psi_j(\zeta,\tau)$ $(j=+,0,-)$ responsible for spin-independent and spin-dependent collisions between identical spin-1 bosons, taking the form $b_0=\pi\hbar^2(a_0+2a_2)/3m$ and $b_2=\pi\hbar^2(a_2-a_0)/3\mathrm{m}$ where a_0 and a_2 represent the s-wave scattering lengths within the symmetric channels characterized by the total spin of the colliding atoms, $F=0$ and $F=2$, respectively [54–56].

In this paper, considering the transformation $(\Psi_+,\Psi_0,\Psi_-)\rightarrow(\psi_+,\sqrt{2}\,\psi_0,\psi_-)$, $x=\zeta\sqrt{2\mathrm{m}}/\hbar$, $t=\tau/\hbar$, the dimensionless three-component GPEs are formed as:

$$\begin{aligned}
\mathrm{i}\partial_t\psi_+ =& -\partial_x^2\psi_+ + U_+(x)\psi_+ + (c_0+c_2)(|\psi_+|^2+2|\psi_0|^2)\psi_+\\
&+(c_0-c_2)|\psi_-|^2\psi_+ + 2c_2\psi_0^2\psi_-^*,\\
\mathrm{i}\partial_t\psi_0 =& -\partial_x^2\psi_0 + U_0(x)\psi_0 + (c_0+c_2)(|\psi_+|^2\\
&+|\psi_-|^2)\psi_0 \quad + \quad 2c_0|\psi_0|^2\psi_0 \quad + \quad 2c_2\psi_0^*\psi_+\psi_-,\\
\mathrm{i}\partial_t\psi_- =& -\partial_x^2\psi_- + U_-(x)\psi_- + (c_0+c_2)(|\psi_-|^2+2|\psi_0|^2)\psi_-\\
&+(c_0-c_2)|\psi_+|^2\psi_- + 2c_2\psi_0^2\psi_+^*,
\end{aligned} \tag{2}$$

where $U_j(x)=V_j(x)+\mathrm{i}W_j(x)$ $(j=+,0,-)$ is the $\mathcal{PT}$-symmetric generalized Scarf-II potential [57, 58] which can modulate the degree of the energy distribution of matter-wave solitons presented under the external potential well and $W_j(x)$ $(j=+,0,-)$ represents the gain-and-loss distribution. Since the introduction of the concept of $\mathcal{PT}$-symmetry, achieving a balance between gain and loss in quantum systems has been a long-standing goal in quantum mechanics, and it has only recently been realized experimentally [59]. Such $\mathcal{PT}$-symmetric Scarf-II potentials in a spinor BEC can possibly be realized by creating arbitrary optical potentials in time average [60] and also the experimental realization of localized loss [61–63] and of localized gain [64]. The concrete forms of the $\mathcal{PT}$-symmetric generalized Scarf-II potential are shown as:

$$\begin{aligned}
V_j(x) &= v_j\,\mathrm{sech}^2(x) + \alpha_j\,\mathrm{sech}^{2n}(x),\\
W_j(x) &= w_j\,\mathrm{sech}(x)\tanh(x), \quad j=+,0,-,
\end{aligned} \tag{3}$$

with v_j, α_j, w_j $(j=+,0,-)$, and $n>0$ being all real-valued potential parameters, which can modulate the structure of $\mathcal{PT}$-symmetric potential. Clearly, when $\alpha_j=0$ or $n=1$ $(v_j+\alpha_j\neq 0, j=+,0,-)$, the complex potential (3) transforms into the classical Scarf-II potential [65–67]. As the case of $c_0=c_2<0$ has been investigated in the references [68, 69], yielding analytical solutions of equations (1) under $\mathcal{PT}$-symmetric Scarf-II potential and $\mathcal{PT}$-symmetric harmonic-Hermitian-Gaussian potential, along with results on different types of soliton collisions, this paper primarily focuses on the scenarios where $c_2=0.1$ (antiferromagnetic) and $c_2=-0.5$ (ferromagnetic) under $\mathcal{PT}$-symmetric generalized Scarf-II potentials.

The subsequent sections of this paper are organized as follows. In section 2, we explore the soliton states of equations (2), obtaining its families of analytical soliton states under $\mathcal{PT}$-symmetric generalized Scarf-II potentials. We conduct linear stability analysis, distinguishing stable and unstable regions. The results are validated through dynamic evolution with 5% perturbations. In section 3, we utilize the power-conserving squared-operator methods [44] to generate families of numerical soliton states for equations (2). A detailed investigation of points on the curves is carried out, obtaining the evolution of corresponding stable and unstable numerical solitons. Some analytical soliton states, numerical single-hump soliton states, and numerical double-hump soliton states are chosen to interact with exotic Gaussian solitons. Finally, our conclusions are presented in section 4.

2. Analytical soliton states

With the stationary states transformation $\psi_j(x,t)=\phi_j(x)\mathrm{e}^{\mathrm{i}\mu_j t}$ $(j=+,0,-)$, the three-component GPEs can be derived as

$$\begin{aligned}
&-\mu_+\phi_+ + \phi_+'' - [V_+(x)+\mathrm{i}W_+(x)]\phi_+ - (c_0+c_2)(|\phi_+|^2\\
&+2|\phi_0|^2)\phi_+ - (c_0-c_2)|\phi_-|^2\phi_+ - 2c_2\phi_0^2\phi_-^* = 0,\\
&-\mu_0\phi_0 + \phi_0'' - [V_0(x)+\mathrm{i}W_0(x)]\phi_0 - (c_0+c_2)(|\phi_+|^2\\
&+|\phi_-|^2)\phi_0 - 2c_0|\phi_0|^2\phi_0 - 2c_2\phi_0^*\phi_+\phi_- = 0,\\
&-\mu_-\phi_- + \phi_-'' - [V_-(x)+\mathrm{i}W_-(x)]\phi_- - (c_0+c_2)(|\phi_-|^2\\
&+2|\phi_0|^2)\phi_- - (c_0-c_2)|\phi_+|^2\phi_- - 2c_2\phi_0^2\phi_+^* = 0,
\end{aligned} \tag{4}$$

where μ_j $(j=+,0,-)$ represents the real chemical potential. For obtaining the soliton states of equations (4), we utilize the

constraints $w_+ + w_- = 2w_0$, $\mu_+ = \mu_0 = \mu_- = n^2$, $A_0^2 = A_+A_-$, $\alpha_+ = \alpha_0 = \alpha_-$,

$$v_j = -\left(\frac{w_j}{2n+1}\right)^2 - n^2 - n, \qquad j = +, 0, -,$$

and derive

$$\begin{aligned} &\phi_j(x) = A_j \,\mathrm{sech}^n(x)\, \mathrm{e}^{\mathrm{i}\theta_j(x)}, \\ &\theta_j(x) = -\frac{2w_j}{2n+1}\arctan\left(\tanh\frac{x}{2}\right), \qquad j = +, 0, -, \\ &A_+ + A_- = \sqrt{\frac{\alpha_+}{-(c_0+c_2)}}. \end{aligned} \tag{5}$$

To demonstrate the stability of soliton states, we perform the linear stability analysis on the obtained soliton solutions $\psi_j(x, t)$ $(j = +, 0, -)$ of Equation (2). Substituting the perturbed solutions ($\epsilon \ll 1$)

$$\begin{aligned} \psi_j(x, t) = \phi_j(x)\mathrm{e}^{\mathrm{i}\mu_j t} + \epsilon[f_j(x)\mathrm{e}^{\mathrm{i}\delta t} \\ + g_j^*(x)\mathrm{e}^{-\mathrm{i}\delta^* t}]\mathrm{e}^{\mathrm{i}\mu_j t}, \quad j = +, 0, -, \end{aligned} \tag{6}$$

into equations (2) yields an eigenvalue problem $\boldsymbol{LY} = \delta\boldsymbol{Y}$, where δ stands for the eigenvalue, $f_j(x)$, $g_j(x)$ $(j = +, 0, -)$ are components of the corresponding eigenfunction, $\boldsymbol{Y} = (f_1, g_1, f_2, g_2, f_3, g_3)^{\mathrm{T}}$, and the specific form of $\boldsymbol{L}$ is shown in appendix.

For the given eigenvalue problem, we discretize the differential operator into a matrix using spectral methods [70, 71] and obtain the numerical values for δ. Considering the inherent errors in numerical methods, when the maximum of $|\mathrm{Im}(\delta)|$ is sufficiently small ($|\mathrm{Im}(\delta)| < 10^{-5}$), δ can be approximated as a real number. In this case, the solutions $\psi_j(x, t)$ $(j = +, 0, -)$ can be considered linearly stable. This theoretical assumption is further validated through numerical evolution with 5% perturbations.

As a result, when we choose the system parameters as $c_0 = 1$, $c_2 = -0.5$, the curve of analytical soliton family for n concerning the atomic densities of soliton can be obtained, as illustrated in figure 1(a1). The atomic densities are defined as $P_j = \int|\psi_j(x)|^2\,\mathrm{d}x$ $(j = +, 0, -)$, and the energy flux can be described by introducing the Poynting vector $S_j = \mathrm{i}(\phi_j\phi_{j,x}^* - \phi_j^*\phi_{j,x})/2$ $(j = +, 0, -)$ [72]. Due to constraints on the system parameters for analytical soliton states, only scenarios under the special condition where $P_+ = P_0 = P_- = P$ are studied in this paper. Through linear stability analysis, we distinguish the stable and unstable portions of the curve. The unstable regions are indicated by the red dashed lines, while the stable regions are represented by the blue solid lines. We select one point from each of the stable and unstable sections on the curve for further investigation. Point A in figure 1(a1) is selected from the unstable region, corresponding to $P = 1.6000$ and $n = 0.5$. In figure 1(b1)–(b3), we present its evolutionary results after undergoing 5% perturbations as initial conditions and the corresponding eigenvalue distribution is reflected in figure 1(b4). Point B in figure 1(a1) is chosen from the stable region, with $P = 0.8000$ and $n = 1.5$. Similarly, in figure 1(c1)-(c4), we illustrate its evolutionary results with 5% perturbations, along with the corresponding eigenvalue distribution. Clearly, the soliton states corresponding to point A is unstable, while that of point B is stable, confirming the accuracy of linear stable analysis. Moreover, we observe that as the value of n increases from 0.5 to 1.5, the atomic density decreases by just half, with α_j remaining constant and $|v_j|$ $(j = +, 0, -)$ increasing. This suggests that higher values of $|v_j|$ $(j = +, 0, -)$ may correspond to more stable soliton states.

When the value of c_2 is changed from -0.5 to 0.1, the curve of the obtained analytical solution family exhibit the same shape and position, but the stable region is significantly enlarged, as shown in figure 1(a2). From the curve in figure 1(a2), we select point C with the same coordinates as point A for further investigation. In figure 1(d1)-(d4), we present its evolutionary results after undergoing 5% perturbations as initial conditions and the corresponding eigenvalue distribution. However, the evolution corresponding to point C is stable, indicating that increasing c_2 from -0.5 to 0.1 can decrease the value of α_j, and smaller α_j $(j = +, 0, -)$ values may correspond to stable solitons.

3. Numerical soliton states

Obtaining the analytical solution of equations (2) demands stringent system parameter specifications, rendering the implementation of BECs experiments challenging. Consequently, to surmount these limitations and manipulate the propagation coefficient, numerical methods are employed in our research endeavors.

In our numerical investigation, we first focus on the case when $c_0 = 1$ and $c_2 = -0.5$. With the system parameters chosen as $w_j = 2.5$, $v_j = -3.8$, and $\alpha_j = -0.4$ $(j = +, 0, -)$, we present families of single-hump numerical soliton states in figure 2(a1)-(a3). Clearly, as n grows, the entire curve relocates towards smaller μ values. We further investigate points D and E selected from the curves shown in figure 2(a1)-(a3). Point D corresponds to $P_+ = 3.6600$, $P_0 = 4.6321$, $P_- = 5.3079$, $\mu_+ = 1.8563$, $\mu_0 = 1.8555$, $\mu_- = 1.8571$; point E corresponds to $P_+ = 4.0000$, $P_0 = 5.0624$, $P_- = 4.5376$, $\mu_+ = 1.8724$, $\mu_0 = 1.7685$, $\mu_- = 2.0890$. By performing linear stability analysis on the soliton states corresponding to these three points, we ascertain that the soliton states corresponding to point D is stable, and the stability of the soliton states corresponding to point E is unstable. Similarly, we validate these findings by conducting numerical evolution with 5% perturbations.

Next, we investigate the numerical families of double-hump soliton states when $c_0 = 1$ and $c_2 = 0.1$. Given the constancy of other conditions, the numerical double-hump solution families across various n values exhibit significant overlap, hence in figure 3, we only show the scenario for $n = 2$. We change the values of w_j from 2.5 to 0.8, v_j from -3.8 to -6, while keeping the values of α_j $(j = +, 0, -)$ unchanged. Similarly, we further investigate points F and G selected from the curves shown in figure 3(a1)-(a3). Figure 3(b1)-(b4) and figure 3(d1)-(d4) depict the progression of stable soliton states respectively, along with their associated eigenvalue distributions. Of note, as shown in

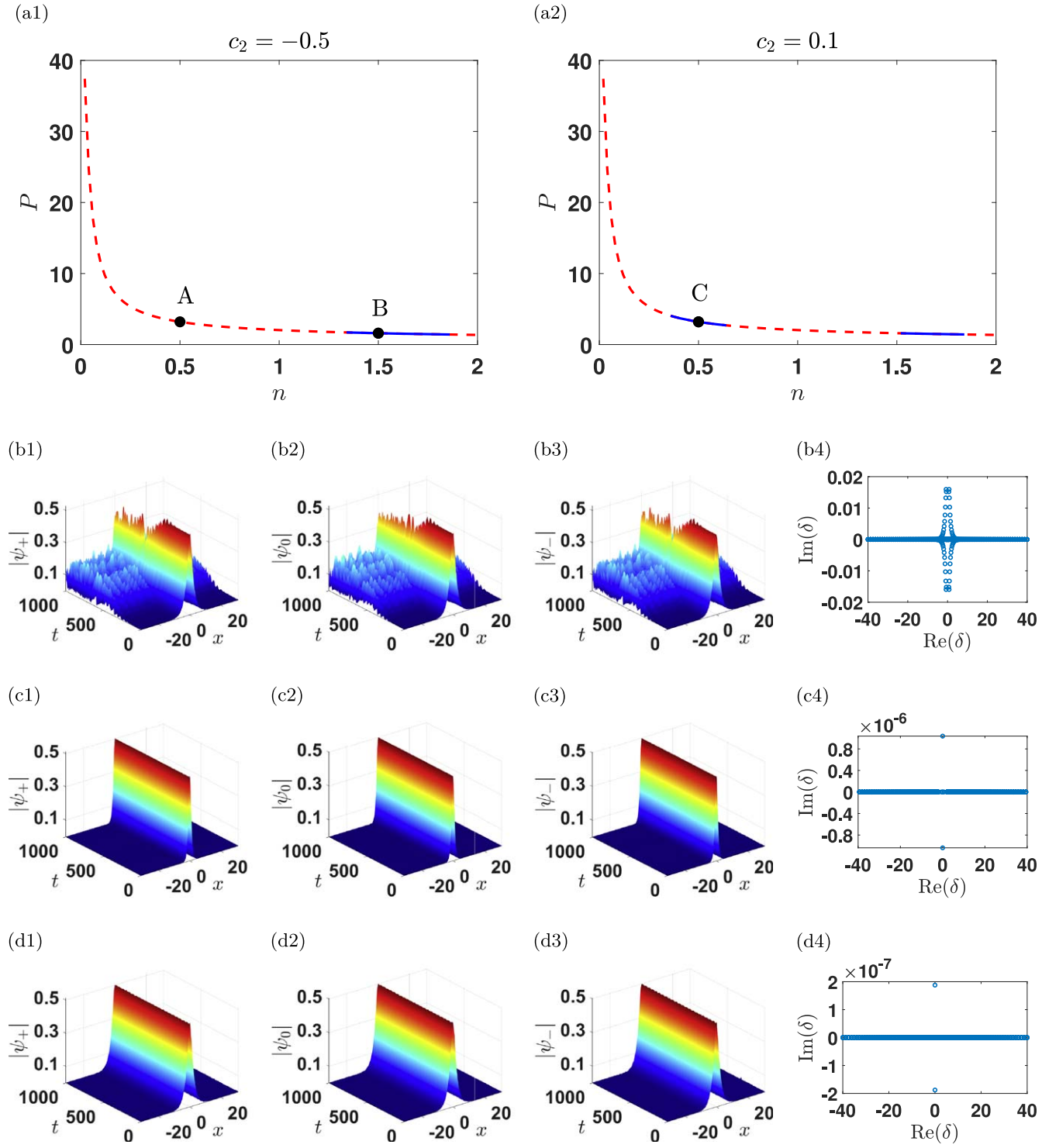

Figure 1. Families of analytical soliton states, the progression of stable/unstable analytical solitons and their eigenvalues for linear stability, associated with $c_2 = -0.5$ and $c_2 = 0.1$ respectively. The parameters are chosen as: $c_0 = 1$, $w_j = 0.6$, $A_j = 0.5$ ($j = +, 0, -$). (b1)-(b4) correspond to point A in (a1) where $v_j = -0.8400$, $\alpha_j = -0.5$ ($j = +, 0, -$) and $P = 1.6000$, $n = 0.5$. (c1)-(c4) correspond to point B in (a1) where $v_j = -3.7725$, $\alpha_j = -0.5$ and $P = 0.8000$, $n = 1.5$. (d1)-(d4) correspond to point C in (a2) where $v_j = -0.8400$, $\alpha_j = -1.1$ ($j = +, 0, -$) and $P = 1.6000$, $n = 0.5$.

figure 3(b1)-(b3), the double-hump soliton states corresponding to point F exhibit periodic oscillations while conserving the energy during propagation, which can be seen as a form of energy exchange between soliton states. Furthermore, compared to previous studies where all three soliton states exhibited periodic oscillations, the phenomenon of energy exchange only existing between ψ_+ and ψ_0, with ψ_- remaining constant, might be relatively infrequent. To further investigate the oscillatory behavior of the double-hump soliton states, the total number energy flux from the numerical solutions is investigated. Point G from figure 3(a1)-(a3) is selected for study, compared to point F, the corresponding oscillation period is longer, and ψ_- also

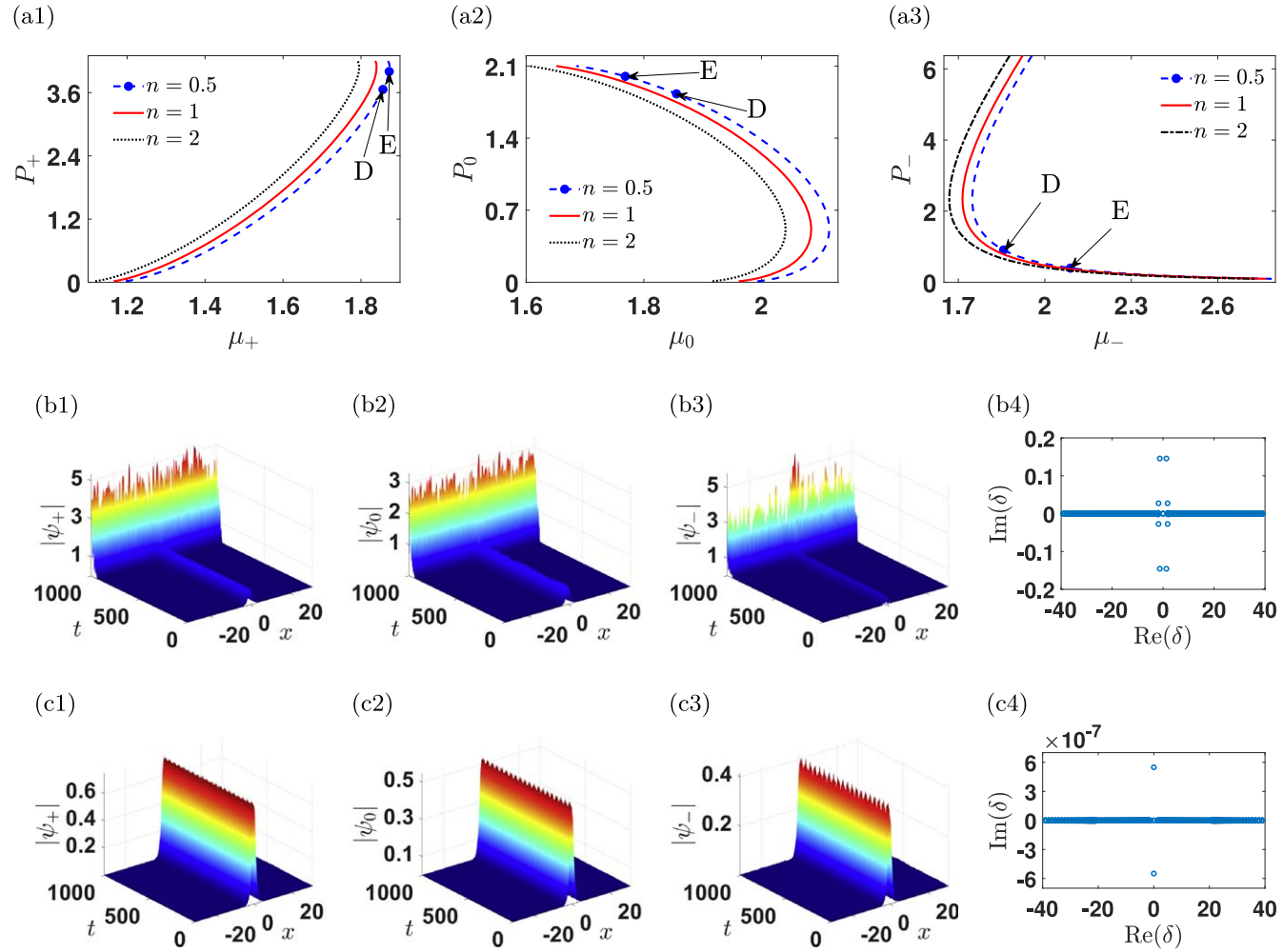

Figure 2. Families of numerical single-hump soliton states, the progression of stable/unstable numerical single-hump solitons and their eigenvalues for linear stability, associated with different n. The parameters are chosen as: $c_0 = 1$, $c_2 = -0.5$, $w_+ = w_0 = w_- = 2.5$, $v_+ = v_0 = v_- = -3.8$, $\alpha_+ = \alpha_0 = \alpha_- = -0.4$.

begins to exhibit slight oscillations, as shown in figure 3(c1)-(e4). This suggests that the oscillation of the double-hump soliton states may be related to the magnitude of the energy and indicates the dynamic stability of the double-hump soliton against small perturbations.

Next, we turn our attention to studying the interaction between Gaussian solitons and the solitons depicted in figure 1 to figure 3. We consider the following initial conditions

$$\overline{\psi_j}(x,0) = \psi_j(x,0) + q_j e^{-0.05(x+23)^2+3ix} + q_j e^{-0.05(x-23)^2-3ix}, \quad j = +, 0, -, \tag{7}$$

and

$$\overline{\psi_j}(x,0) = \psi_j(x,0) + q_j e^{-0.05(x+23)^2+4ix} + q_j e^{-0.05(x-23)^2-4ix}, \quad j = +, 0, -, \tag{8}$$

where q_j is the maximum amplitude of the exotic Gaussian soliton. Figure 4(a1)-(a3) correspond to the case of analytical solitons with $c_0 = 1$, $c_2 = -0.5$, $n = 0.5$, $w_j = 0.6$, $A_j = 0.5$, $P = 1.6000$, $v_j = -3.7725$, and $\alpha_j = -0.5$ ($j = +$, 0, $-$), satisfying the initial condition (7); figure 4(b1)-(b3) correspond to the case of numerical single-hump solitons (point D) with $P_+ = 3.6600$, $P_0 = 4.6321$, $P_- = 5.3079$, $\mu_+ = 1.8563$, $\mu_0 = 1.8555$, $\mu_- = 1.8571$, $\mu_0 = 1.7329$, $\mu_- = 1.7262$, and $n = 0.5$, satisfying the initial condition (7); figure 4(c1)-(c3) correspond to the case of numerical double-hump solitons (point F) with $P_+ = 0.0400$, $P_0 = 0.0506$, $P_- = 13.5547$, $\mu_+ = 0.7273$, $\mu_0 = 0.6493$, $\mu_- = 0.6556$, and $n = 2$, satisfying the initial condition (7); figure 4(d1)-(d3) correspond to the case of numerical double-hump solitons (point G) with $P_+ = 0.3200$, $P_0 = 0.4050$, $P_- = 12.8750$, $\mu_+ = 0.7083$, $\mu_0 = 0.6319$, $\mu_- = 0.6497$, and $n = 2$, satisfying the initial condition (8). For figure 4(a1)-(a3), we choose $q_+ = q_0 = q_- = 0.2$, for figure 4(b1)-(b3), we choose $q_+ = q_0 = 0.05$, $q_- = 0.3$, while for figure 4(d1)-(d3), we choose $q_+ = q_0 = 0.1$, $q_- = 0.5$. We notice that after the interaction between the stable soliton states and the exotic Gaussian solitons, both of them maintain their original shapes and continue to propagate forward, as shown in

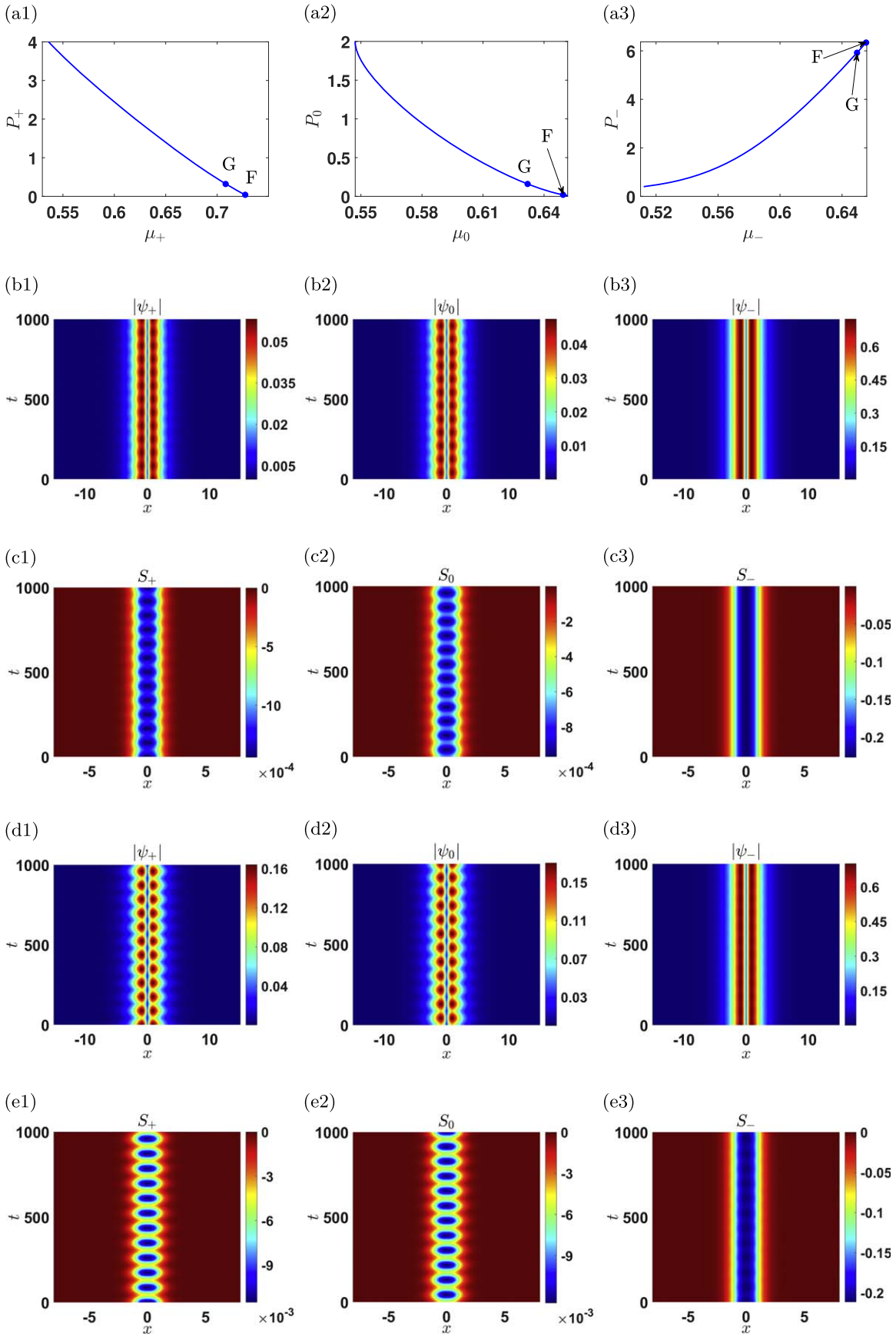

Figure 3. Families of numerical double-hump soliton states, the progression of stable numerical double-hump solitons and their energy flux associated with $n = 2$. The parameters are chosen as: $c_0 = 1$, $c_2 = 0.1$, $w_+ = w_0 = w_- = 0.8$, $v_+ = v_0 = v_- = -6$, $\alpha_+ = \alpha_0 = \alpha_- = -0.4$. And their maximum of $|\mathrm{Im}(\delta)|$ for linear stability are all 10^{-7}.

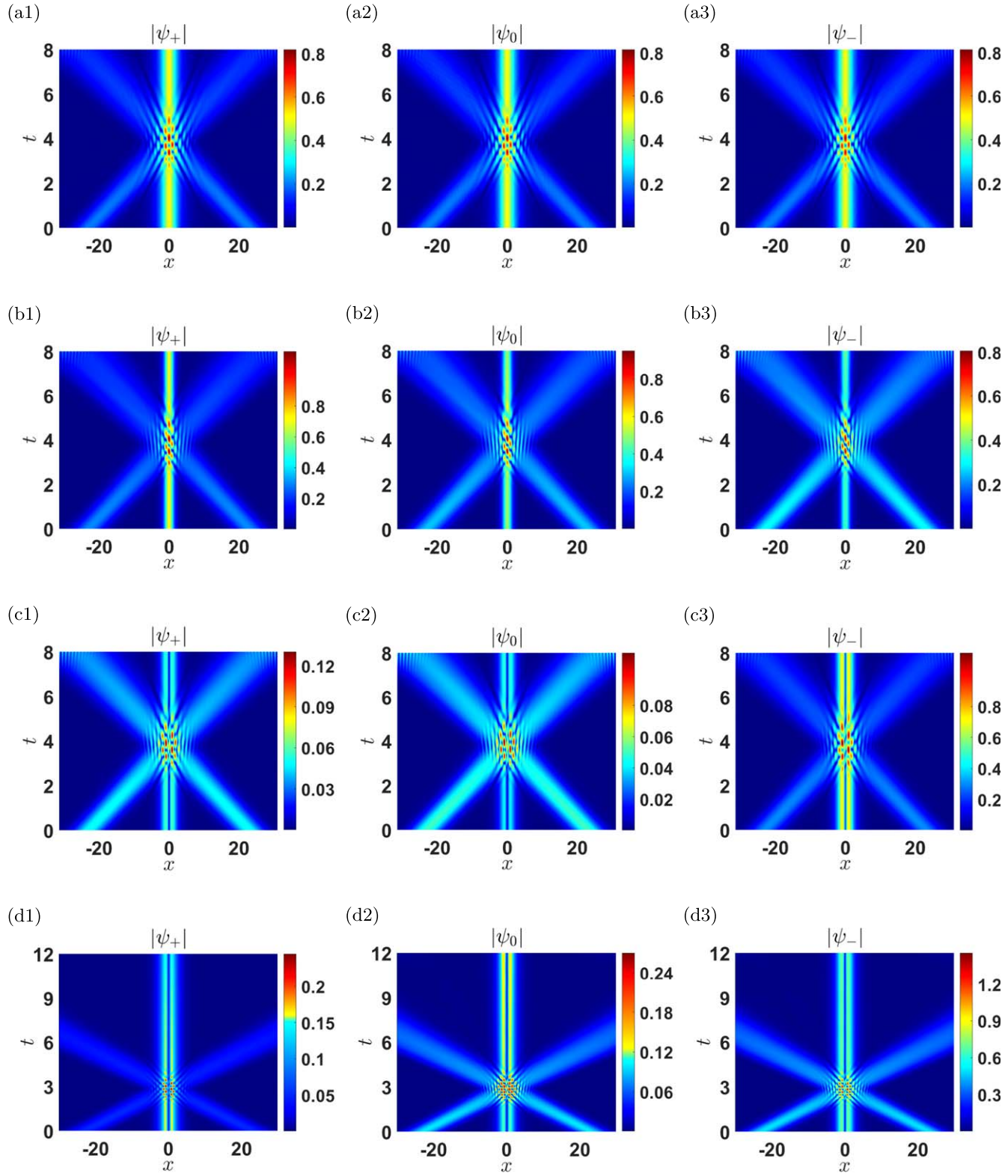

Figure 4. Interactions of single-hump and double-hump soliton states with exotic Gaussian solitons. (a1)-(a3) correspond to analytical soliton states at $c_0 = 1$, $c_2 = -0.5$, $n = 0.5$, $w_j = 0.6$, $A_j = 0.5$, $P = 1.6000$, $v_j = -3.7725$ and $\alpha_j = -0.5$ ($j = +, 0, -$). (b1)-(b3) correspond to numerical single-hump soliton states at $n = 0.5$. (c1)-(d3) correspond to numerical double-hump soliton states at $n = 2$.

figure 4(a1)-(c3). This indicates that an elastic collision occurs between the soliton states and the exotic Gaussian solitons. Moreover, some studies suggest that interactions between solitons may trigger energy flow among the three components. However as shown in figure 4(d1)-(d2), we observe a specific scenario where the energy of ψ_+ decreases, and the energy of ψ_0 increases, while the energy of ψ_- remains unchanged after the interaction between the exotic

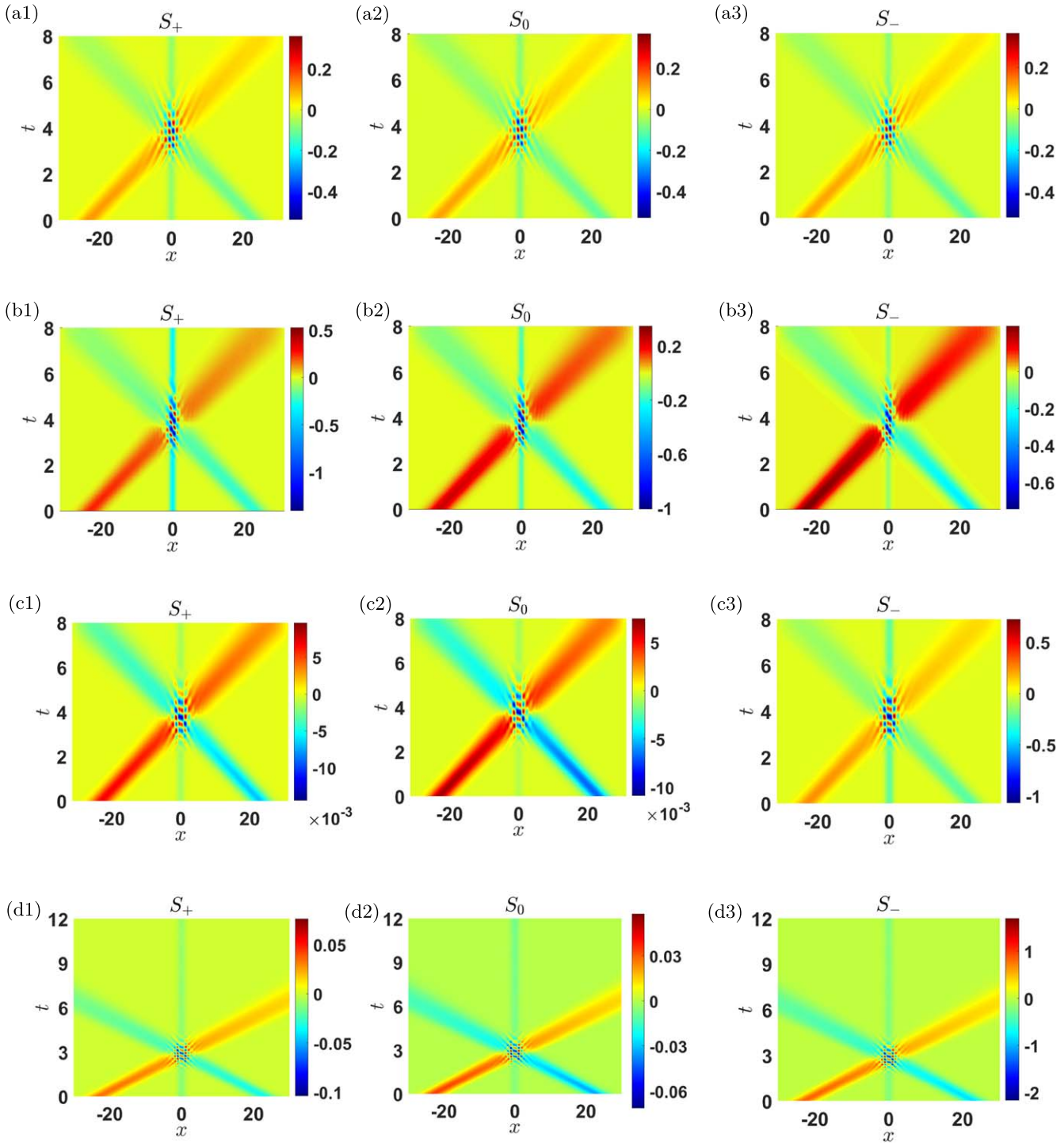

Figure 5. The energy flux of the interactions of single-hump and double-hump soliton states with exotic Gaussian solitons in figure 4. The parameters are chosen the same as figure 4.

Gaussian solitons and the double-hump solitons. This can be regarded as a special form of energy flow involving only two components. In order to explore more properties about the interaction, the corresponding energy flux are checked. As illustrated in figure 5, the Poynting vectors of $\psi_j(x, t)$ all keep invariant. Moreover, the energy flux of the soliton states has the same characteristics as that $\psi_j(x, t)$ propagate, which further verifies the correctness of figure 4.

4. Conclusions

In conclusion, we introduce $\mathcal{PT}$-symmetric generalized Scarf-II potentials into three-coupled Gross–Pitaevskii equations with two different scenarios of inter-component interaction parameter values c_0 and c_2, and obtain corresponding analytical/numerical soliton states and soliton families. In both scenarios of parameter configurations, the

analytical soliton families exhibit identical curve shapes, but the stable region of the analytical soliton family curves significantly increases under the condition of $c_2 = 0.1$. With the condition of $c_2 = -0.5$ (ferromagnetic), the single-hump solution families obtained through iterative algorithms shift towards smaller values of μ as n increases. Besides, in the case of $c_2 = 0.1$ (antiferromagnetic), we obtain point F whose corresponding double-hump soliton states exhibit periodic oscillations while conserving the energy during propagation, within the double-hump soliton families. Notably, the phenomenon of energy exchange only existing between ψ_+ and ψ_0, with ψ_- remaining constant, is observed. Moreover, after the interaction between the double-hump soliton states and the exotic Gaussian solitons, the energy of ψ_+ decreases and the energy of ψ_0 increases, while the energy of ψ_- unchanged. This phenomenon can be seen as collisions triggering the flow of energy among the three components. These findings could contribute to a deeper understanding of solitons in Bose–Einstein condensates with $\mathcal{PT}$-symmetric potentials and potentially aid in designing relevant physics experiments.

Acknowledgments

We express our sincere thanks to the editor, referees, and all the members of our discussion group for their valuable comments. This work was supported by NSFC under Grant No. 12272403, and Beijing Training Program of Innovation under Grant No. S202410019024. The funding body plays an important role in the design of the study, in analysis, calculation, and in writing of the manuscript.

Declarations of interest

The authors declare that they have no conflict of interest.

Appendix

The matrix $\boldsymbol{L}$ of the linear eigenvalue problem, which is derived during linear stability analysis, has a specific form as follows:

$$\boldsymbol{L} = \begin{pmatrix} L_1 & L_{12} & L_{13} & L_{14} & L_{15} & L_{16} \\ L_{21} & -L_1^* & L_{23} & L_{24} & L_{25} & L_{26} \\ L_{31} & L_{32} & L_2 & L_{34} & L_{35} & L_{36} \\ L_{41} & L_{42} & L_{43} & -L_2^* & L_{45} & L_{46} \\ L_{51} & L_{52} & L_{53} & L_{54} & L_3 & L_{56} \\ L_{61} & L_{62} & L_{63} & L_{64} & L_{65} & -L_3^* \end{pmatrix}, \tag{9}$$

where

$$\begin{aligned}
L_1 &= \partial_x^2 - 2(c_0 + c_2)\phi_+\phi_+^* - 2(c_0 + c_2)\phi_0\phi_0^* \\
&\quad - (c_0 - c_2)\phi_-\phi_-^* - U_+(x) - \mu_+, \\
L_2 &= \partial_x^2 - (c_0 + c_2)\phi_+\phi_+^* - 4c_0\phi_0\phi_0^* \\
&\quad - (c_0 + c_2)\phi_-\phi_-^* - U_0(x) - \mu_0, \\
L_3 &= \partial_x^2 - (c_0 - c_2)\phi_+\phi_+^* - 2(c_0 + c_2)\phi_0\phi_0^* \\
&\quad - 2(c_0 + c_2)\phi_-\phi_-^* - U_-(x) - \mu_-, \\
L_{12} &= -(c_0 + c_2)\phi_+^2, \\
L_{14} &= -2(c_0 + c_2)\phi_+\phi_0, \\
L_{15} &= -(c_0 - c_2)\phi_+\phi_-^*, \\
L_{21} &= (c_0 + c_2)\phi_+^{*2}, \\
L_{23} &= 2(c_0 + c_2)\phi_+^*\phi_0^*, \\
L_{26} &= (c_0 - c_2)\phi_+^*\phi_-, \\
L_{32} &= -(c_0 + c_2)\phi_+\phi_0, \\
L_{36} &= -(c_0 + c_2)\phi_0\phi_-, \\
L_{41} &= (c_0 + c_2)\phi_+^*\phi_0^*, \\
L_{45} &= (c_0 + c_2)\phi_0^*\phi_-^*, \\
L_{51} &= -(c_0 - c_2)\phi_+^*\phi_-, \\
L_{54} &= -2(c_0 + c_2)\phi_0\phi_-, \\
L_{56} &= -(c_0 + c_2)\phi_-^2, \\
L_{62} &= (c_0 + c_2)\phi_+\phi_-^*, \\
L_{63} &= 2(c_0 + c_2)\phi_0^*\phi_-^*, \\
L_{65} &= (c_0 + c_2)\phi_-^{*2}, \\
L_{13} &= -2(c_0 + c_2)\phi_+\phi_0^* + 4c_2\phi_0\phi_-^*, \\
L_{16} &= -(c_0 - c_2)\phi_+\phi_- - 2c_2\phi_0^2, \\
L_{24} &= 2(c_0 + c_2)\phi_+^*\phi_0 + 4c_2\phi_0^*\phi_-, \\
L_{25} &= (c_0 - c_2)\phi_+^*\phi_-^* + 2c_2\phi_0^{*2}, \\
L_{31} &= -(c_0 + c_2)\phi_+^*\phi_0 - 2c_2\phi_0^*\phi_-, \\
L_{34} &= -2c_0\phi_0^2 - 2c_2\phi_+\phi_-, \\
L_{35} &= -(c_0 + c_2)\phi_0\phi_-^* - 2c_2\phi_+\phi_0^*, \\
L_{42} &= (c_0 + c_2)\phi_+\phi_0^* + 4c_2\phi_0\phi_-^*, \\
L_{43} &= 2c_0\phi_0^{*2} + 2c_2\phi_+^*\phi_-^*, \\
L_{46} &= (c_0 + c_2)\phi_0^*\phi_- + 2c_2\phi_+^*\phi_0, \\
L_{52} &= -(c_0 - c_2)\phi_+\phi_- - 2c_2\phi_0^2, \\
L_{53} &= -2(c_0 + c_2)\phi_0^*\phi_- - 4c_2\phi_+^*\phi_0, \\
L_{61} &= (c_0 - c_2)\phi_+^*\phi_-^* + 2c_2\phi_0^{*2}, \\
L_{64} &= 2(c_0 + c_2)\phi_0\phi_-^* + 4c_2\phi_+\phi_0^*.
\end{aligned}$$

References

[1] Lerario G *et al* 2017 Room-temperature superfluidity in a polariton condensate *Nat. Phys.* **13** 837–41
[2] Stamper-Kurn D M and Ueda M 2013 Spinor Bose gases: symmetries, magnetism, and quantum dynamics *Rev. Mod. Phys.* **85** 1191

[3] Yulin A V *et al* 2011 Superfluidity of Bose–Einstein condensates in toroidal traps with nonlinear lattices *Phys. Rev.* A **84** 063638

[4] Alexandrov A S 1998 *d*-wave Bose–Einstein condensate and tunnelling in superconducting cuprates *Physica* C **305** 46–56

[5] Sun M *et al* 2021 Bose–Einstein condensate-mediated superconductivity in graphene *2D Mater* **8** 031004

[6] Huang Y X *et al* 2015 Quantum entanglement in a spin-orbit coupled Bose–Einstein condensate *Commun. Theor. Phys.* **64** 644

[7] Yu Z X, Jiao Z Y and Sun J Z 2004 Quantum effects of Bose–Einstein condensates *Commun. Theor. Phys.* **41** 593

[8] Zhu H G, Shu J, Huang G Q and Luo C L 2014 Coherence and entanglement in spinor Bose–Einstein condensate *Int. J. Theor. Phys.* **53** 2803–9

[9] Stamper-Kurn D M *et al* 1998 Optical confinement of a Bose–Einstein condensate *Phys. Rev. Lett.* **80** 2027–30

[10] Hung N V, Szankowski P, Konotop V V and Trippenbach M 2020 Four-wave mixing in spin-orbit coupled Bose–Einstein condensates *New. J. Phys.* **22** 053019

[11] Liu T and Liew T C H 2017 Spontaneous spin bifurcations in a Bose–Einstein condensate of indirect excitons *Superlattice. Microst.* **108** 57–63

[12] Hoshi S and Saito H 2008 Magnetization of a half-quantum vortex in a spinor Bose–Einstein condensate *Phys. Rev.* A **78** 053618

[13] Zhang J M *et al* 2009 Probing the quantum ground state of a spin-1 Bose–Einstein condensate with cavity transmission spectra *Phys. Rev.* A **80** 043623

[14] Isoshima T and Yip S 2006 Effect of quadratic Zeeman energy on the vortex of spinor Bose–Einstein condensates *J. Phys. Soc. Jpn.* **75** 074605

[15] Sandoval-Santana J C, Zamora-Zamora R, Paredes R and Romero-Rochín V 2021 Intrinsic decoherence and recurrences in a large ferromagnetic $F = 1$ spinor Bose–Einstein condensate *Symmetry* **13** 67

[16] Zhao D *et al* 2015 Topological defects and inhomogeneous spin patterns induced by the quadratic Zeeman effect in spin-1 Bose–Einstein condensates *Phys. Rev.* A **91** 013619

[17] Kevrekidis P G, Theocharis G, Frantzeskakis D J and Malomed B A 2003 Feshbach resonance management for Bose–Einstein condensates *Phys. Rev. Lett.* **90** 230401

[18] Yan M *et al* 2013 Controlling condensate collapse and expansion with an optical Feshbach resonance *Phys. Rev. Lett.* **110** 123201

[19] Enomoto K, Kasa K, Kitagawa M and Takahashi Y 2008 Optical feshbach resonance using the intercombination transition *Phys. Rev. Lett.* **101** 203201

[20] Shen Y J *et al* 2014 Nonautonomous matter waves in a spin-1 Bose–Einstein condensate *Phys. Rev.* E **89** 062915

[21] Zhang X F, Hu X H, Liu X X and Liu W M 2009 Vector solitons in two-component Bose–Einstein condensates with tunable interactions and harmonic potential *Phys. Rev.* A **79** 033630

[22] Rajendran S, Muruganandam P and Lakshmanan M 2010 Bright and dark solitons in a quasi-1D Bose–Einstein condensates modelled by 1D Gross–Pitaevskii equation with time-dependent parameters *Physica* D **239** 366–86

[23] Yao Y Q, Han W, Li J and Liu W M 2018 Localized nonlinear waves and dynamical stability in spinor Bose–Einstein condensates with time-space modulation *J. Phys.* B **51** 105001

[24] Dast D, Haag D, Cartarius H and Wunner G 2016 Purity oscillations in Bose–Einstein condensates with balanced gain and loss *Phys. Rev.* A **93** 033617

[25] Dast D, Haag D, Cartarius H and Wunner G 2014 Quantum master equation with balanced gain and loss *Phys. Rev.* A **90** 052120

[26] Lunt P, Haag D, Dast D, Cartarius H and Wunner G 2017 Balanced gain and loss in Bose–Einstein condensates without $\mathcal{PT}$-symmetry *Phys. Rev.* A **96** 023614

[27] Bender C M 2007 Making sense of non-Hermitian Hamiltonians *Rep. Prog. Phys.* **70** 947

[28] Bender C M, Brody D C and Jones H F 2003 Must a Hamiltonian be Hermitian? *Am. J. Phys.* **71** 1095–102

[29] Bender C M and Boettcher S 1998 Real spectra in non-Hermitian Hamiltonians having $\mathcal{PT}$-symmetry *Phys. Rev. Lett.* **80** 5243

[30] Lao J Y, Qin Z Y, Zhang J R and Shen Y J 2024 Peakons in spinor $F = 1$ Bose–Einstein condensates with $\mathcal{PT}$-symmetric δ-function potentials *Chaos Solitons Fractals* **180** 114497

[31] Makris K G, El-Ganainy R, Christodoulides D N and Musslimani Z H 2008 Beam dynamics in $\mathcal{PT}$-symmetric optical lattices *Phys. Rev. Lett.* **100** 103904

[32] Longhi S 2009 Bloch oscillations in complex crystals with $\mathcal{PT}$-symmetry *Phys. Rev. Lett.* **103** 123601

[33] Feng L *et al* 2011 Nonreciprocal light propagation in a silicon photonic circuit *Science* **333** 729–33

[34] Regensburger A *et al* 2012 Parity-time synthetic photonic lattices *Nature* **488** 167–71

[35] Cartarius H and Wunner G 2012 Model of a $\mathcal{PT}$-symmetric Bose–Einstein condensate in a δ-function double-well potential *Phys. Rev.* A **86** 013612

[36] Hiller M, Kottos T and Ossipov A 2006 Bifurcations in resonance widths of an open Bose–Hubbard dimer *Phys. Rev.* A **73** 063625

[37] Lee J M, Kottos T and Shapiro B 2015 Macroscopic magnetic structures with balanced gain and loss *Phys. Rev.* B **91** 094416

[38] Galda A and Vinokur V M 2016 Parity-time symmetry breaking in magnetic systems *Phys. Rev.* B **94** 020408

[39] Fleury R, Sounas D and Alù A 2015 An invisible acoustic sensor based on parity-time symmetry *Nat. Commun.* **6** 5905

[40] Shi C *et al* 2016 Accessing the exceptional points of parity-time symmetric acoustics *Nat. Commun.* **7** 11110

[41] Bender N *et al* 2013 Observation of asymmetric transport in structures with active nonlinearities *Phys. Rev. Lett.* **110** 234101

[42] Bagarello F 2013 From self-adjoint to non-self-adjoint harmonic oscillators: physical consequences and mathematical pitfalls *Phys. Rev.* A **88** 032120

[43] Yang J K 2014 Necessity of $\mathcal{PT}$-symmetry for soliton families in one-dimensional complex potentials *Phys. Lett.* A **378** 367–73

[44] Yang J K 2010 *Nonlinear Waves in Integrable and Nonintegrable Systems* (Philadelphia, PA: SIAM)

[45] Klaiman S, Günther U and Moiseyev N 2008 Visualization of branch points in $\mathcal{PT}$-symmetric waveguides *Phys. Rev. Lett.* **101** 080402

[46] Xu Y X *et al* 2023 Rydberg-dressed solitons in Bose–Einstein condensates with parity-time symmetry *Results in Physics* **49** 106534

[47] Kartashov Y V, Konotop V V and Abdullaev F K 2013 Gap solitons in a spin-orbit-coupled Bose–Einstein condensate *Phys. Rev. Lett.* **111** 060402

[48] Bhatia S, Goyal A, Jana S and Kumar C N 2023 Stationary hypergeometric solitons and their stability in a Bose–Einstein condensate with $\mathcal{PT}$-symmetric potential *Phys. Lett.* A **469** 128751

[49] Ho T L 1998 Spinor Bose condensates in optical traps *Phys. Rev. Lett.* **81** 742

[50] Kawaguchi Y and Ueda M 2012 Spinor Bose–Einstein condensates *Phys. Rep.* **520** 253–381

[51] Ohmi T and Machida K 1998 Bose–Einstein condensation with internal degrees of freedom in alkali atom gases *J. Phys. Soc. Jpn.* **67** 1822–5

[52] Pethick C J and Smith H 2008 *Bose–Einstein Condensation in Dilute Gases*. (Cambridge: Cambridge University Press)
[53] Zhang Z H, Zhang C, Yang S J and Feng S 2012 Analytical solutions to the spin-1 Bose–Einstein condensates *J. Phys.* B **45** 215302
[54] Dabrowska-Wüster B J, Ostrovskaya E A, Alexander T J and Kivshar Y S 2007 Multicomponent gap solitons in spinor Bose–Einstein condensates *Phys. Rev.* A **75** 023617
[55] Martikainen J P, Collin A and Suominen K A 2002 Coreless vortex ground state of the rotating spinor condensate *Phys. Rev.* A **66** 053604
[56] Nistazakis H E *et al* 2008 Bright-dark soliton complexes in spinor Bose–Einstein condensates *Phys. Rev.* A **77** 033612
[57] Chen Y, Yan Z Y and Malomed B A 2022 Higher-dimensional soliton generation, stability and excitations of the $\mathcal{PT}$-symmetric nonlinear Schrödinger equations *Physica* D **430** 133099
[58] Chen Y, Yan Z Y and Mihalache D 2020 Soliton formation and stability under the interplay between parity-time-symmetric generalized Scarf-II potentials and Kerr nonlinearity *Phys. Rev.* E **102** 012216
[59] Altinisik S, Dizdarevic D and Main J 2019 Balanced gain and loss in spatially extended non-$\mathcal{PT}$-symmetric multiwell potentials *Phys. Rev.* A **100** 063639
[60] Henderson1 K, Ryu1 C, MacCormick C and Boshier M G 2009 Experimental demonstration of painting arbitrary and dynamic potentials for Bose–Einstein condensates *New J. Phys.* **11** 043030
[61] Gericke T *et al* 2008 High-resolution scanning electron microscopy of an ultracold quantum gas *Nature Phys* **4** 949–53
[62] Würtz P *et al* 2009 Experimental demonstration of single-site addressability in a two-dimensional optical lattice *Phys. Rev. Lett.* **103** 080404
[63] Barontini G *et al* 2013 Controlling the dynamics of an open many-body quantum system with localized dissipation *Phys. Rev. Lett.* **110** 035302
[64] Döring D *et al* 2009 Pulsed pumping of a Bose–Einstein condensate *Phys. Rev.* A **79** 063630
[65] Shen Y J, Wen Z C, Yan Z Y and Hang C 2018 Effect of $\mathcal{PT}$-symmetry on nonlinear waves for three-wave interaction models in the quadratic nonlinear media *Chaos* **28** 043104
[66] Ahmed Z 2001 Real and complex discrete eigenvalues in an exactly solvable one-dimensional complex $\mathcal{PT}$-invariant potential *Phys. Lett.* A **282** 343–48
[67] Musslimani Z H, Makris K G, El-Ganainy R and Christodoulides D N 2008 Optical solitons in $\mathcal{PT}$ periodic potentials *Phys. Rev. Lett.* **100** 030402
[68] Qi J J, Zhao D and Liu W M 2023 Soliton collisions in spin-orbit coupled spin-1 Bose–Einstein condensates *J. Phys. A: Math. Theor.* **56** 255702
[69] Zhong M, Yan Z Y and Tian S F 2023 Stable matter-wave solitons, interactions, and excitations in the spinor $F = 1$ Bose–Einstein condensates with $\mathcal{PT}$-and non-$\mathcal{PT}$-symmetric potentials *Commun. Nonlinear Sci. Numer. Simul.* **118** 107061
[70] Shen J, Tang T and Teng Z 2006 *Spectral and High-Order Methods with Applications* (Shanghai: Science Press)
[71] Trefethen L N 2000 *Spectral Methods in MATLAB* (Philadelphia, PA: SIAM)
[72] Barashenkov I V, Zezyulin D A and Konotop V V 2016 Jamming anomaly in $\mathcal{PT}$-symmetric systems *New J. Phys.* **18** 075015